

Facile synthesis of heterostructure CeO₂/CdS and CdS/CeO₂ nanocomposites for photocatalytic application of methylene blue textile dye

G. Murugadoss^{a,*}, M. R. Kumar^b, A. Kathalingam^c, J. R. Rajabathar^{d,*},
H. Al-Lohedan^d, D. M. Al-Dhayan^d

^aCentre for Nanoscience and Nanotechnology, Sathyabama Institute of Science and Technology, Chennai 600119, Tamil Nadu, India

^bInstitute of Natural Science and Mathematics, Ural Federal University, Yekaterinburg 620002, Russia

^cMillimeter-wave Innovation Technology Research Center, Dongguk University-Seoul, Seoul 04620, Republic of Korea

^dDepartment of chemistry, College of science, King Saud University, PO Box 2455, Riyadh 11451, Kingdom of Saudi Arabia

Heterostructure CeO₂/CdS and CdS/CeO₂ nanocomposites were synthesized by a facile 'one-pot' chemical method in ambient atmosphere and examined photocatalytic activity. The as-prepared nanocomposites were characterized using XRD, SEM, TEM, UV-vis, PL and TG-DTA. The obtained results reveal successful formation of CeO₂/CdS and CdS/CeO₂ nanocomposites. The TEM images show that well-dispersed particles were uniform and fairly small, mainly spherical-like shape. Enhanced photocatalytic degradation efficiency was observed for CdS/CeO₂ composite exhibits 86%. This result suggested that the CdS/CeO₂ composite significantly improve the photocatalytic efficiency due to reduction the recombination of photogenerated electron-hole pairs and creation of efficient free radicals. This work could provide a novel approach to construct new heterojunction photocatalysts and a deeper insight for the treatment of textile wastewater.

(Received October 4, 2021; Accepted December 21, 2021)

Keywords: Nanocomposites, Chemical method, Methylene blue, Photocatalytic activity

1. Introduction

Metal Oxide and Metal Sulfide based nanocomposites are very popular and useful in various applications, such as photocatalysis, photonics, electronics and drug delivery [1, 2]. Tremendous research works on metal oxides such as TiO₂, CeO₂, ZnS, WO₃, V₂O₅, SnO₂, CdS, etc have been reported for various energy and environmental applications [3–6]. CdS is a predictable narrow band-gap (direct band gap of 2.42 eV) semiconductor and is currently under investigation owing to its tremendous applications in response to its tunable properties. particularly, it has been extensively studied in photocatalytic hydrogen production due to its ability in harvesting visible light and suitable conduction band potential [7]. However, the utility of alone CdS has been limited due to its anodic decomposition (photocorrosion) [8]. Recently, the optical, catalytic and electrical properties of CdS have been modified by adding suitable rare earth metal or metal oxides, [5–12] but investigations of CdS with rare-earth oxides heterostructures are limited. Thus, it is highly desirable to investigate the properties of CdS with rare earth oxide heterostructures for diverse applications.

The extensive research carried out on n-n type junction semiconductor systems, particularly, the CeO₂-based nanocomposites such as CeO₂/Fe₂O₃ [17], CeO₂/ZnO [18], CeO₂@NiO [19], CeO₂/TiO₂ [20], CeO₂/ZrO₂ [21], CeO₂@ α -MoO₃ [22], CeO₂/Bi₂O₃ [23], CeO₂/CrO [24], CeO₂/SnO₂ [25], CeO₂/SrTiO₃ [26], CeO₂/Ag-AgCl [27], CeO₂/BiVO₄ [28], (CeO₂, La₂O₃, C)/TiO₂ [29], CeO₂/Co [30] and so on for photocatalytic and energy conversion

* Corresponding author: jrajabathar@ksu.edu.sa

applications. The results showed that nearly all the n–n junction semiconductor materials exhibited better photocatalytic properties than single compound.

In this work, CeO₂/CdS and CdS/CeO₂ nanocomposites were prepared and studied using various characterization techniques including X-ray diffraction (XRD), scanning electron microscopy (SEM), UV–vis and Photoluminescence and Thermogravimetry and differential thermal analysis. The CeO₂/CdS and CdS/CeO₂ nanocomposites were applied to the photocatalytic degradation of MB dye under visible light irradiation. The obtained results showed excellent photocatalytic activities.

2. Experimental details

2.1. Materials

To synthesize CdS/CeO₂ and CeO₂/CdS nanocomposites, the following materials were used. The chemical reagents used were analytical reagent grade without further purification. Cadmium acetate (Cd(CH₃COO)₂·2H₂O), Cerium acetate Ce(NO₃)₃·6H₂O, Sodium sulfide (Na₂S), Sodium hydroxide (NaOH) obtained from Nice Chemical company, Kochi, India were used as precursors. All the glassware used in this experimental work were acid washed. Ultra pure water was used for dilution and sample preparation.

2.2. Synthesis of heterostructure CeO₂/CdS and CdS/CeO₂ nanocomposites

The heterostructure CeO₂/CdS nanocomposite was synthesized by chemical precipitation method. First, 0.1 M of Ce(NO₃)₃·6H₂O was dissolved in 50 ml of de-ionized water under stirring at 80°C temperature. Then, 1.0 g of PVP was added into the above solution. After 10 min, 0.3 M of NaOH was added drop wise into the above aqueous solution. The mixture was again stirred for 1 h. Then, 0.1 M concentrations of 50 mL cadmium acetate aqueous solution was added to the above colloidal solution. Next, 1 M of sodium sulfide solution in 25 ml was added drop wise into the mixture solution and then the resultant solution was stirred for additional 2 h. After the reaction was completed, the solution was cooled down to room temperature. The precipitate was collected and washed with ethanol and acetone for several times. Subsequently, the prepared product was dried at 120 °C for 12 h and then the final product was used for further characterization. The same experimental procedure was followed for the synthesis of heterostructure CdS/CeO₂ nanocomposites by addition the precursors inversely.

2.3. Photocatalytic degradation of MB dye under UV-visible light irradiation

The photocatalytic activities of CdS/CeO₂ and CeO₂/CdS nanocomposites were evaluated for the degradation of MB dye in aqueous solution under natural sun light irradiation. In a typical experiment, a 50 mg of (CdS/CeO₂) was dispersed into 50 mL of MB dye solution. At certain irradiation time interval, 5 mL of the suspension was collected and then centrifuged (6000 rpm, 10 min) to separate the photocatalyst particles. Finally, the irradiated solution was filtered and UV measurements was carried out for determine photodegradation. The same photocatalytic method was used for the CeO₂/CdS nanocomposites.

2.4. Characterization

The crystal structure of the products were determined by X-ray diffraction (XRD) pattern using an X'pert PRO diffractometer with CuK α radiation ($\lambda=1.54060\text{\AA}$) at room temperature. The nanocomposite morphology and size were evaluated from TEM (Technai20G2, FEI). The optical transmission/absorption spectra of the particles in de-ionized water were recorded using a UV-1650PC SHIMADZU spectrophotometer. Fluorescence measurements were performed on a RF-5301PC Spectrophotometer. Thermogravimetric and differential thermal analysis (TG-DTA) were studied using a SDT Q600 20 thermometer in air at heating rate of 10 °C/min.

3. Results and Discussion

XRD pattern of CeO₂/CdS nanocomposites are displayed in Fig. 1a. The main diffraction peaks of CeO₂ are marked by asterisks (*) and CdS is marked by (◆). The diffraction peaks at 28.548°, 33.083°, 47.486°, 56.345°, 59.092° and 69.418° are corresponds to the (1 1 1), (2 0 0), (2 2 0), (2 2 2) and (4 0 0) planes. The sharp and more intense peaks are well matched with cubic structure of CeO₂ (JCPDS No. 89-8436) and the diffraction peaks at 24.929°, 26.66°, 28.328°, 36.821°, 43.905°, 48.117° and 67.164° are corresponds to (1 0 0), (0 0 2), (1 0 1), (1 0 2), (1 1 0), (1 0 3) and (2 0 3) planes of hexagonal structure of CdS (JCPDS No. 80-0006). Fig. 1b shows the XRD pattern of CdS/CeO₂ nanocomposites, where diffraction peaks of cubic CeO₂ are exist at (1 1 1), (2 0 0), (2 2 0), (3 1 1), (2 2 2), (4 0 0) and (3 3 1), the peaks are marked by asterisks (*). Moreover, the other diffraction peaks such as (1 0 0), (0 0 2), (1 0 1), (1 0 2), (1 1 0), (1 0 3) and (2 0 3) marked by (◆) symbol corresponding to hexagonal structure belonged to the CdS nanoparticles. No impurity peaks were observed, it obviously shows high purity of the nanocomposites. The present result is agreement with the reported results [33]. The crystalline size was calculated by using Debye Scherer formula [34],

$$D = (K\lambda) / (\beta \cos\theta) \quad (1)$$

where λ is a wavelength of X-ray radiation, β is a full width at half maximum (FWHM) of the peaks at the diffracting angle (θ). All diffraction peaks observed in both CeO₂/CdS and CdS/CeO₂ nanocomposites. The crystallite size of the nanocomposites were found that 21.6 and 23.4 nm for CeO₂/CdS and CdS/CeO₂ nanocomposites, respectively.

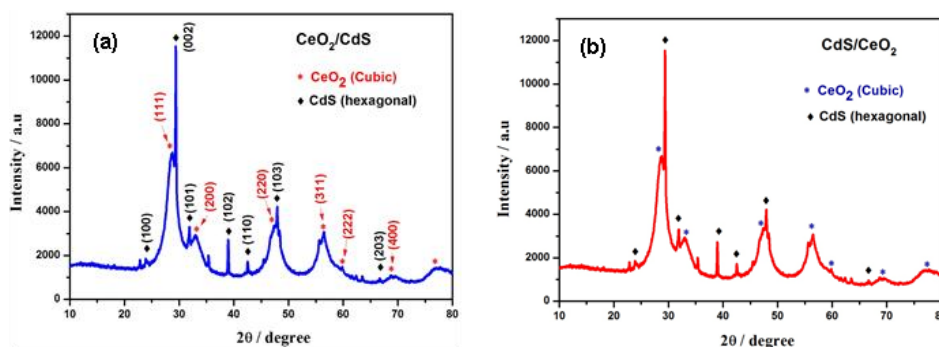


Fig. 1. XRD spectra of the (a) CdS/CeO₂ and (b) CeO₂/CdS nanocomposites.

Fig. 2 shows typical SEM images of different magnifications of the synthesized heterostructure CeO₂-CdS (a, b) and CdS-CeO₂ (c, d) nanocomposites. The SEM images showed distinct variation of the morphology by revert the two compounds in the nanocomposites. Two different morphologies showed that cubic and 2D based plat like structure. To further investigate the morphology, TEM study was carried out and the result is shown in Fig. 3(a&b). The morphology of CeO₂-CdS clearly showed that the particles were uniform and fairly small, mainly spherical-like shape with diameters of 20-30 nm range, which are consistent with observation from XRD patterns.

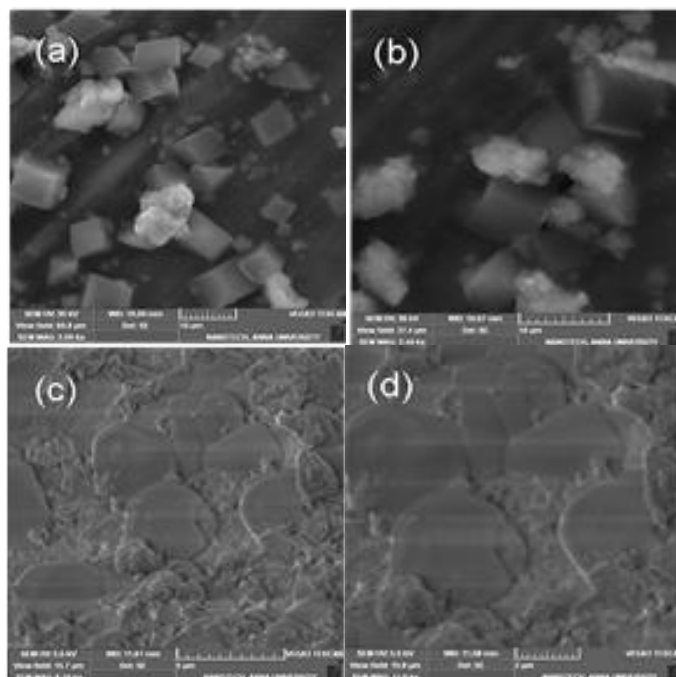


Fig. 2. SEM images of different magnifications of (a, b) heterostructure CeO_2/CdS and (c, d) CdS/CeO_2 nanocomposites.

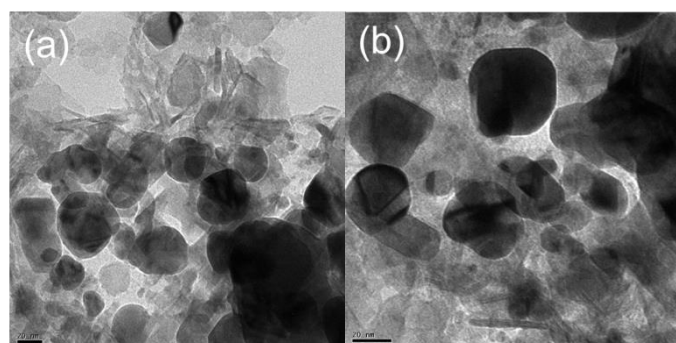


Fig. 3. (a, b) TEM images of the heterostructure CeO_2/CdS nanocomposites with various magnifications.

Fig. 4a shows the UV-vis absorbance spectra of CeO_2/CdS and CdS/CeO_2 nanocomposites synthesized by a co-precipitation method. It is clearly observed that the absorption peak appeared at around 360 nm and 380 nm, respectively. Compared with pure CeO_2 and CdS compounds, the nanocomposites demonstrated red shifting absorption. The red shifting and narrow band gap composite facilitate to absorb wide range of light. In addition, the red shifting absorption can be support to enhance photocatalytic performance. The UV spectrum originates from transition between S^{2-} and Ce^{4+} . This indicates that transition overlaps with $4f^1-5d^1$ transition of Ce^{3+} ions [35]. On the other hand, the UV spectrum may be attributed from the transition between O^{2-} and Cd^{2+} . The significant shifting observed in the UV absorption by simply exchange the CeO_2 and CdS compounds. The absorption result is clearly demonstrated the necessity of the preparation of sulfide and oxide combined composite and exchanging the compounds. Fig. 4b shows that the energy bandgap curve which obtained from Tauc plot. The following formula is used to calculate the energy bandgap (E_g) [36]:

$$\alpha(h\nu) = A(h\nu - E_g)^{n/2} \quad (2)$$

where ' α ' and ' $h\nu$ ' represent the absorption coefficient and the light energy, ' A ' is a constant, ' E_g ' the optical bandgap and n is an integer equal to 1 for a direct bandgap and 4 for an indirect bandgap. The plot of $(\alpha h\nu)^2$ versus Energy (eV) was used for estimating the value of bandgap energy of CeO₂/CdS and CdS/CeO₂ nanocomposites by extrapolating curve to zero absorption, the obtained result is displayed in Fig. 4b. The estimated value of the bandgap (E_g) was found to be 3.21 and 3.42 eV for CeO₂/CdS and CdS/CeO₂ nanocomposites, respectively. The optical bandgap of CeO₂/CdS nanocomposite increases slightly compared to the CdS/CeO₂ nanocomposite. It is evident that significant blue shift of the absorption peak relative to the bulk absorption. The blue shift of the absorption peak may be related to the quantum size effect which arises due to very small size of the nanocomposites.

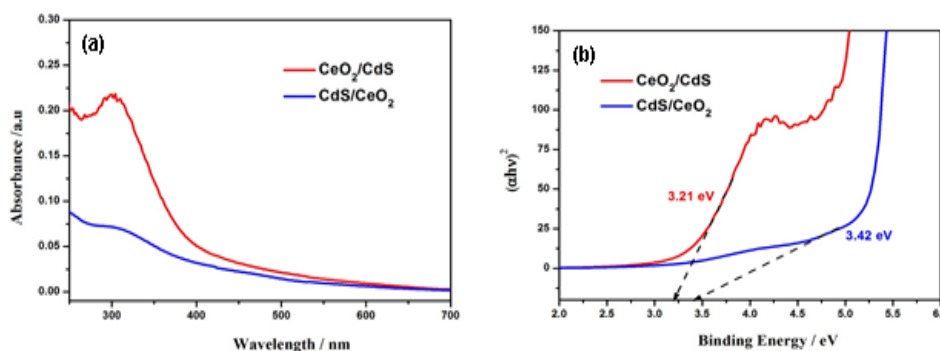


Fig. 4. (a) UV/visible and (b) Tauc plot spectra of the overlapped CdS/CeO₂ and CeO₂/CdS nanocomposites, respectively.

Photoluminescence spectra of CeO₂/CdS and CdS/CeO₂ nanocomposites are shown in Fig. 5. It shows a broad band between 350-500 nm for the both nanocomposites. The broad PL band indicates that this defect-related luminescence peak is caused by radiative transitions between Cd and Ce interstitials acting as shallow donors and Cd and Ce vacancies acting as deep acceptors. This recombination mechanism competes with the exciton-related luminescence and seems to depend on the stoichiometry and the preparation conditions [37, 38]. Strong emission showed for CeO₂/CdS than CdS/CeO₂ nanocomposites, it may be high recombination of charge carriers on the binary CeO₂/CdS system.

The degree of crystallization and decompose of residual organic molecules was studied by the TG-DTA measurement. Fig. 6(a-b) shows the TG-DTA curves of CeO₂-CdS and CdS-CeO₂ nanocomposites, the samples were heated from room temperature to 1000 °C with an increment of 10 °C/min in air atmosphere. In the Fig. 6a and Fig. 6b, the endothermic peak at low temperature corresponds to a clear weight loss on the TG curve, which is caused by the evaporation of physically adsorbed water on the surface of the precursor. Fig. 6a, shows weight loss occurs in the two stages. The first step is associated with a weight loss on the TG curve within the temperature range of 50–260 °C (endothermic), which mainly occurs owing to the elimination of adsorbed water in the crystalline sample. The second step of weight loss on the TG curve within the temperature range of 260–800 °C (endothermic) and corresponding changes observed in same temperature range in the DTA curve. A broad exothermic peak showed around at 400 °C, which can be correlated to the oxidative decarboxylation of CeO_x to CeO₂. Fig. 6b shows a gradual weight loss on the TG curve within the temperature range of 50–234 °C (endothermic), which mainly occurs owing to the elimination of adsorbed water. Further heating (900-1000°C), both the samples are highly stable. This confirms that the formation of well oxidated CeO₂ and CdO [39].

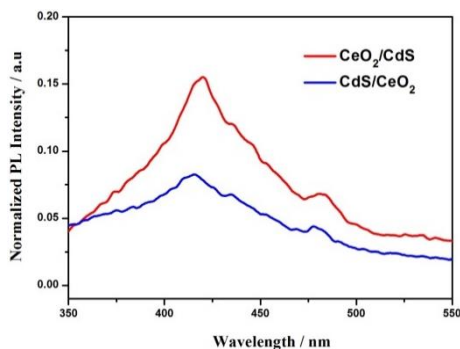


Fig. 5. Photoluminescence spectra of the CdS/CeO₂ and CeO₂/CdS nanocomposites.

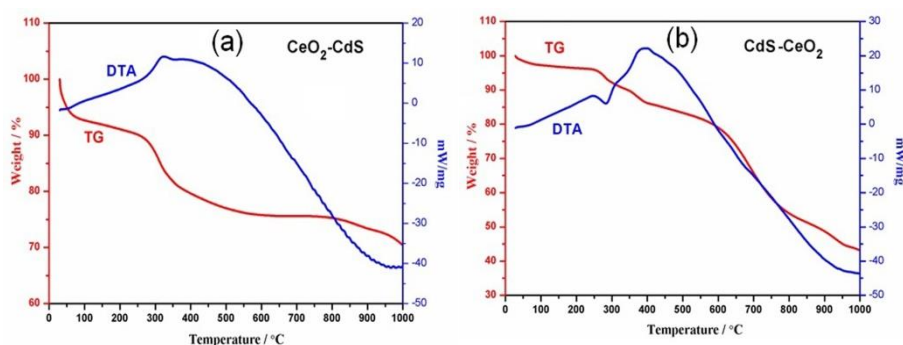


Fig. 6 TG-DTA of the (a) CeO₂/CdS and (c) CdS/CeO₂ nanocomposites. The samples were annealed at nitrogen atmosphere from RT to 1000 °C.

In order to examine photocatalytic activity of the nanocomposites, the samples were used as catalyst for the degradation of MB dye. In general, the organic dyes can be photodegraded via three possible reactions including photosensitization, photolysis, and photocatalysis [40]. Figure 7(a-b) shows the UV absorbance of MB aqueous solution collected at a regular time interval (30 mins) for CeO₂/CdS and CdS/CeO₂ composites under visible light irradiation. The degradation was calculated using C/C_0 , where C_0 is the initial concentration and C is the concentration after photo-irradiation with respect to degradation time as shown in Fig. 7(c-d). Fig. 7c shows the photocatalytic degradation efficiency of the both nanocomposites. As shown in Fig. 7b, it is evident that the CdS/CeO₂ composites exhibited higher photocatalytic activities than CeO₂/CdS, this may due to narrow band gap and suitable band gap alignment. Enhanced photocatalytic degradation efficiency of 86% was achieved for CdS/CeO₂ composite. This photocatalytic improvement is higher than the reported metal oxide-based composites [41-43]. This result suggested that the CdS/CeO₂ composite significantly improve the photocatalytic efficiency by reducing recombination of photogenerated electron-hole pairs. The obtained result is good agreement with optical study. Furthermore, the corresponding pseudo-first-order rate law was plotted as a function of visible irradiation time according to the following linear equation [44]:

$$-\ln(C/C_0) = kt \quad (3)$$

where C_0 and C are the initial and residual concentrations of MB aqueous solution, time t (min). The calculated apparent rate constant (k , min⁻¹) was labelled in Fig. 7(e), which is acquired from the slope drawn from the plot of $-\ln(C/C_0)$ versus time (t). As demonstrated in Fig. 7(e), the degradation rate constant of CdS/CeO₂ was calculated as 0.01011 min⁻¹ presenting the highest photocatalytic performance compared to CeO₂/CdS (0.00424 min⁻¹). The enhanced photocatalytic activity of the CdS/CeO₂ nanocomposite was mainly due to (i) the encumbrance of the electron-hole recombination process due to the separation of photogenerated charge carriers between CeO₂

and CdS and (ii) the enhancement of light absorption ability of CdS/CeO₂ composite in the visible region.

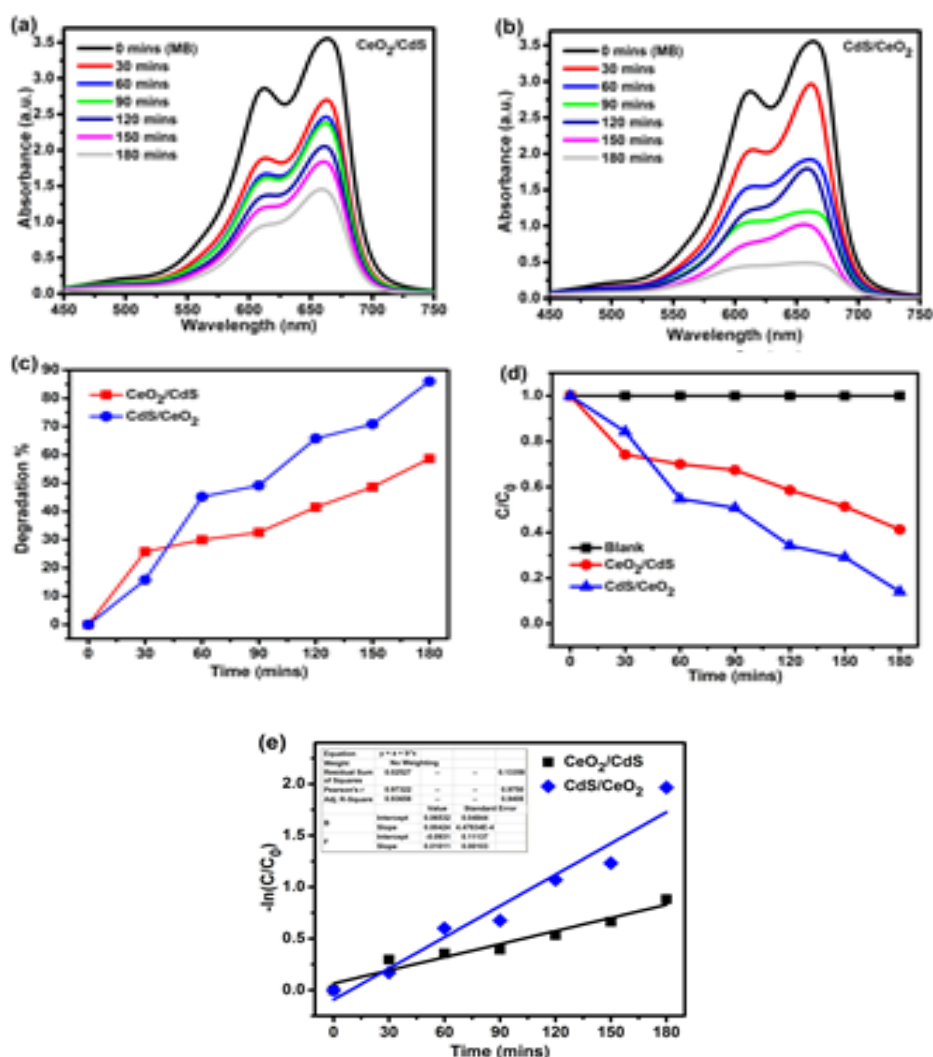


Fig. 7. (a, b) UV-vis spectra of the CeO₂/CdS and CdS/CeO₂ nanocomposites dispersed in methylene blue dye solution with light irradiation of different time interval, respectively. (c) Percentage of the dye degradation versus time interval. (d, e) (C/C₀) versus time interval and Plot of $-\ln(C/C_0)$ versus time interval, respectively.

The most important part is the formation of matching structure from the band edges of CeO₂ and CdS, as shown in Fig. 8. Photoexcited electrons are produced in the conduction band (CB) of CdS under light irradiation and then transfer to the Ce-4f orbital of CeO₂. At the same time, photoexcited holes in the valence band (VB) of CeO₂ move to the VB of CdS, which can facilitate the separation of photoexcited electrons–holes and suppress their recombination, and thus, lead to an improved photocatalytic performance by creation of free radicals [42]. The CdS/CeO₂ absorbs photon energy and then generates photoexcited electrons and holes.

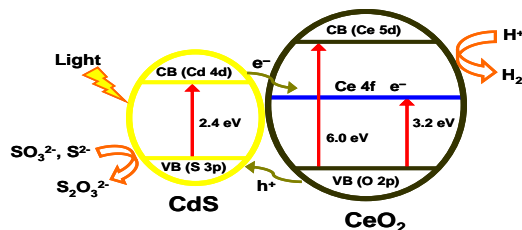


Fig. 8. Photocatalytic degradation mechanism of CeO_2/CdS under visible light irradiation.

4. Conclusions

In summary, heterostructure CeO_2/CdS and CdS/CeO_2 nanocomposites were synthesized directly by a simple ‘one-pot’ chemical method. The mixed structure of Cubic (CeO_2)-Hexagonal (CdS) nanocomposite was determined by XRD analysis. The morphology of the nanocomposites was analyzed using SEM and TEM studies. It was found that mainly spherical-like shape with diameters of 20-30 nm range. Compared with the bare CeO_2 and CdS , the optical absorption of the nanocomposite was noticeably shifted. The tuning optical band gap facilitated to increasing photon absorption, resulting enhanced photocatalytic activity of the MB dye. Thus, this work provides a simple route to prepare CeO_2 -based nanocomposite materials for effective photocatalytic degradation of dye pollutants. The synthesis of nanocomposite may provide a low cost and efficient method for remediation of organic effluents in wastewater in the textile industries.

Acknowledgements

The authors thank for the financial support by the Researchers Supporting Project Number (RSP-2021/354) King Saud University, Riyadh, Saudi Arabia. One of author (Manavalan Rajesh Kumar) thanks to the contract no. 40/is2 and MES of RF (contract no. FEUZ-2020-0051).

References

- [1] X. Hu, G. Li, J.C. Yu, *Langmuir* **26**, 3031 (2010).
- [2] J. Mu, B. Chen, M. Zhang, Z. Guo, P. Zhang, Z. Zhang, Y. Sun, C. Shao, Y. Liu, *Appl. Mater. Interf.* **4**, 424 (2012).
- [3] O. Carp, C.L. Huisman, A. Reller, *Prog. Sol. State Chem.* **32**, 33 (2004).
- [4] G. Murugadoss, J. Ma, X. Ning, M. R. Kumar, *Inorg. Chem. Commun.* **109**, 107577 (2019).
- [5] N. Z. Bao, L. M. Shen, T. Takata, K. Domen, *Chem. Mater.* **20**, 110 (2008).
- [6] M. Rajesh Kumar, G. Murugadoss, *J. Lumin.* **146**, 325 (2014).
- [7] S. Y. Ryu, W. Balcerski, T. K. Lee, M. R. Hoffmann, *J. Phys. Chem. C* **111**, 18195 (2007).
- [8] D. Meissner, R. Memming, B. Kastening, *J. Phys. Chem.* **92**, 3476 (1988).
- [9] G. Murugadoss, R. Thangamuthu, R. Jayavel, M. Rajesh Kumar, *J. Lumin.* **165**, 30 (2015).
- [10] M. Nyk, R. Kumar, T. Y. Ohulchanskyy, E. J. Bergey, P.N. Prasad, *Nano Letters* **8**, 3834 (2008).
- [11] G. Murugadoss, *J. Lumin.* **146**, 430 (2014).
- [12] G. Murugadoss, R. Jayavel, M. Rajesh Kumar, *Indian J. Phys.* **90**, 173 (2016).
- [13] L. Yue, X. M. Zhang, *J. Alloys and Compd.* **475**, 702 (2009).
- [14] L. Truffault, M. T. Ta, T. Devers, K. Konstantinov, V. Harel, C. Simmonard, C. Andreazza, I. P. Nevirkovets, A. Pineau, O. Veron, J.-P. Blondeau, *Mater. Res. Bull.* **45**, 527 (2010).
- [15] D. Zhang, *Transition Metal Chem.* **35**, 689 (2010).
- [16] C. Wang, X. M. Wang, B. Q. Xu, J. C. Zhao, B. X. Mai, P. A. Peng, G. Sheng, J. Fu, *J. Photochem. Photobio. A Chem.* **168**, 47 (2004).
- [17] G.K. Pradhan, K.M. Parida, *Inter. J. Eng. Sci. Tech.* **2**, 53 (2010).

- [18] W. Wu, S. Li, S. Liao, F. Xiang, X. Wu, *Rare Metals* **29**, 149 (2010).
- [19] G. Manibalan, G. Murugadoss, R. Thangamuthu, P. Ragupathy, M. R. Kumar, R. M. Kumar, R. Jayavel, *Inorg. Chem.* **58**, 13843 (2019).
- [20] T. Cai, Y. Liao, Z. Peng, Y. Long, Z. Wei, Q. Deng, *J. Environ. Sci.* **21**, 997 (2009).
- [21] G. R. Rao, H. R. Sahu, *J. Chem. Sci.* **113**, 651 (2001).
- [22] G. Manibalan, G. Murugadoss, R. Thangamuthu, R. M. Kumar, M. R. Kumar, R. Jayavel, *J. Mater. Sci.: Mater. in Electronics* **29**, 13692 (2018).
- [23] L. Li, B. Yan, *J. Non-Crystall. Sol.* **355**, 776 (2009).
- [24] I. Bhati, P. B. Punjabi, S.C. Ameta, *Macedonian J. Chem. Chem. Eng.* **29**, 195 (2010).
- [25] G. Manibalan, G. Murugadoss, R. Thangamuthu, R. M. Kumar, R. Jayavel, M. R. Kumar, *Mater. Res. Exp.* **6**, 075032 (2019).
- [26] S. Song, L. Xu, Z. He, J. Chen, *J. Environ. Sci. Technol.* **41**, 5846 (2007).
- [27] H. Wang, L. Yang, H. Yu, F. Peng, *World J. Nano Sci. Eng.* **1**, 129 (2011).
- [28] N. Wetchakun, S. Chaiwichain, B. Inceesungvorn, K. Pingmuang, S. Phanichphant, A. I. Minett, *ACS Appl. Mater. & Interf.* **4**, 3718 (2012).
- [29] R. Rangel, G. J. L. Mercado, P. Bartolo-Perez, R. Garcí'a, *Sci. Adv. Mater.* **4**, 573 (2012).
- [30] N. S. Arul, D. Mangalaraj, P. C. Chen, N. Ponpandian, P. Meena, Y. Masuda, *J. Sol-Gel Sci. Tech.* **64**, 515 (2012).
- [31] Z. L. Liu, J. C. Deng, J. J. Deng, F. F. Li, *Mater. Sci. Eng. B* **150**, 99 (2008).
- [32] M. H. Habibi, E. Askari, *J. Therm. Anal. Calorim.* **111**, 227 (2013).
- [33] S. Gu, Y. Chen, X. Yuan, H. Wang, X. Chen, Y. Liu, Q. Jiang, Z. Wu, G. Zeng, *RSC Adv.* **5**, 79556 (2015).
- [34] A. L. Patterson, *Phys. Rev.* **56**, 978 (1939).
- [35] A. Elaziouti, N. Laouedj, A. Bekka, R.-N. Vannier, *J. King Saud Univ. – Sci.* **27**, 120 (2015).
- [36] J. Lv, K. Dai, J. Zhang, L. Lu, C. Liang, L. Geng, Z. Wang, G. Yuan, G. Zhu, *Appl. Surf. Sci.* **391**, 507 (2017).
- [37] B. J. Jin, H. S. Woo, S. Im, S. H. Bae, S. Y. Lee, *Appl. Surf. Sci.* **521**, 169 (2001).
- [38] B. Mohanty, K. Sahoo, J. Nayak, *Mater. Res. Exp.* **6**, 0950c5 (2019).
- [39] C. M. Magdalane, K. Kaviyarasu, J. J. Vijaya, B. Siddhardha, B. Jeyaraj, *J. Photochem. Photobio. B: Bio.* **163**, 77 (2016).
- [40] H. Yi, M. Jiang, D. Huang, G. Zeng, C. Lai, L. Qin, C. Zhou, B. Li, X. Liu, M. Cheng, W. Xue, P. Xu, C. Zhang, *J. Taiwan Inst. Chem. Eng.* **93**, 184 (2018).
- [41] N. Wetchakun, S. Chaiwichain, B. Inceesungvorn, K. Pingmuang, S. Phanichphant, A. Minett, J. Chen, *ACS Appl. Mater. Interfaces* **7**, 3718 (2012).
- [42] A. B. Lavand, Y. S. Malghe, S. H. Singh, *Indian J. Eng. Mater. Sci.* **2015**, 1 (2015).
- [43] Z. Li, D. Liu, W. Huang, Y. Sun, S. Li, X. Wei, *Surf. Interface Anal.* **51**, 336 (2019).
- [44] C. G. Silva da, J. L. Faria, *J. Photochem. Photobiol. A Chem.* **155**, 133 (2003).